

Non-standard interactions versus planet-scale neutrino oscillations

Wei-Jie Feng,^{1,*} Jian Tang,^{1,†} Tse-Chun Wang,^{1,‡} and Yi-Xing Zhou^{1,§}

¹*School of Physics, Sun Yat-Sen University, Guangzhou 510275, China*

Abstract

The low-energy threshold and the large detector size of Precision IceCube Next Generation Upgrade (PINGU) can make the study on neutrino oscillations with a planet-scale baseline possible. In this task, we consider the configuration that neutrinos are produced at CERN and detected in the PINGU detector, as a benchmark. We discuss its sensitivity of measuring the size of non-standard interactions (NSIs) in matter, which can be described by the parameter $\epsilon_{\alpha\beta}$ (α and β are flavors of neutrinos). We find that the CERN-PINGU configuration improves $\tilde{\epsilon}_{\mu\mu} \equiv \epsilon_{\mu\mu} - \epsilon_{\tau\tau}$ and $\epsilon_{\mu\tau}$ significantly compared to the next-generation accelerator neutrino experiments. Most of degeneracy problems in the precision measurements can be resolved, except the one for $\tilde{\epsilon}_{\mu\mu} \sim -0.035$. Moreover, we point out that this configuration can also be used to detect the CP violation brought by NSIs. Finally, we compare the physics potential in this configuration to that for DUNE, T2HK and P2O, and find that the CERN-PINGU configuration can significantly improve the sensitivity to NSIs.

I. INTRODUCTION

Since confirming this phenomenon of neutrino oscillations in 1998 [1], we nearly complete the knowledge of this flavour-changing behaviour, which can be described by six oscillation parameters including three mixing angles θ_{12} , θ_{13} and θ_{23} , two mass-square differences Δm_{21}^2 and Δm_{31}^2 , and one Dirac CP violating phase δ with solar, atmospheric, accelerator and reactor neutrino data [2–4]. The rest of problems in neutrino oscillations are if θ_{23} is larger or smaller than 45° , which the sign of Δm_{31}^2 is, if CP is violated and what its value δ is. These problems are expected to be resolved in the next-generation neutrino oscillation experiments, *e.g.* DUNE, T2HK, JUNO, etc. The neutrino oscillation reflects the fact that neutrinos are massive, which conflicts with the massless-neutrino prediction in the standard model (SM). This phenomenon is obviously a key to the door of physics beyond SM (BSM), and reveals that SM is not a complete theory.

Far away in Antarctica, Precision IceCube Next Generation Upgrade (PINGU), an extension of the IceCube Neutrino Observatory, was proposed. In this proposal, the lower energy threshold and the 6-million-ton detector are sketched [5]. Goals of PINGU are to detect atmospheric neutrinos [6, 7], supernova neutrinos [8] and the indirect signal of dark matter (by detecting the self annihilation of WIMP-like dark matter [9]). Moreover, the configuration that PINGU receives neutrino beams from accelerators in the northern hemisphere inspired by CERN to Frejus and J-PARC to HyperKamiokande has been considered and discussed [10].

As we believe that SM is not a complete theory, effects from some exotic interactions are widely discussed, for example, non-standard interactions (NSIs) [11–15], neutrino decays [16–18], nonunitarity [19, 20]. NSIs are

interactions evolving at least one neutrinos and other SM fermions by mediating BSM particles [21, 22]. NSIs may take place in three different parts of neutrino oscillations: at the source, at the detector, and in matter (or NSI matter effects). We describe the size of NSIs by the parameter $\epsilon_{\alpha\beta}^{ff'}$, which is the fraction of the strength of coupling for the NSI to the Fermi constant ($\nu_\alpha + f \rightarrow \nu_\beta + f'$). For those taking place in matter, we use the notation $\epsilon_{\alpha\beta}$, as in these interactions $f = f'$. In recent studies, the Large-Mixing-Angle dark solution (LMA-Dark solution) for NSIs allows that NSI matter effects have a strong impact on neutrino oscillations. This solution predicts $\epsilon_{ee} \simeq -3$ [12, 14]. One of upcoming long baseline accelerator neutrino experiments Deep Underground Neutrino Experiment (DUNE) [23, 24] is expected to have some sensitivity to NSIs in matter. Impacts of NSI matter effects on the precision measurement of oscillation parameters and the expected constraints on NSI parameters for DUNE are widely studied [25–38]. The combined results for $\sin^2 2\theta_{13}$ and NSIs by Daya Bay and T2K experiments were given in Ref. [39]. The current global fits can provide constraints at 95% C.L. on NSI parameters with COHERENT data [14]:

$$\begin{aligned} -0.008 &\leq \epsilon_{ee}^u \leq 0.618 \\ -0.111 &\leq \epsilon_{\mu\mu}^u \leq 0.402 \\ -0.110 &\leq \epsilon_{\tau\tau}^u \leq 0.404 \\ -0.006 &\leq \epsilon_{e\mu}^u \leq 0.049 \\ -0.248 &\leq \epsilon_{e\tau}^u \leq 0.116 \\ -0.012 &\leq \epsilon_{\mu\tau}^u \leq 0.009. \end{aligned}$$

Some possible theoretical models are also proposed to realize sizeable NSIs in matter [40–44].

NSIs in matter can be detected by accelerator neutrino oscillation experiments with non-negligible matter effects. In this paper, we study the planet-scale neutrino oscillations to measure the size of NSI matter effects, by revisiting the configuration of sending a neutrino beam from an accelerator facility in the northern hemisphere such as CERN to a detector in the south pole like PINGU. The CERN-PINGU configuration has

* fengwj7@mail2.sysu.edu.cn

† tangjian5@mail.sysu.edu.cn

‡ wangzejun@mail.sysu.edu.cn

§ zhouyx45@mail2.sysu.edu.cn

a baseline of 11810 km. The difference of this configuration from observatories of atmospheric neutrinos is about neutrino fluxes, which come from a specific direction with the well-controlled timing structure in the CERN-PINGU configuration. As a result, smaller systematic errors and the higher ratio of signals over backgrounds are expected. This super long baseline has four advantages for $\epsilon_{\alpha\beta}$ measurements as follows.

1. The neutrino energy (3 GeV - 20 GeV) is higher than current and future neutrino oscillation experiments. Therefore, larger matter effects are expected, and the detection of ν_τ and $\bar{\nu}_\tau$ is achievable.
2. As neutrinos propagate in a longer baseline, NSI matter effects are expected to be more important. With the help of this 11810 km baseline, the value of NSI parameters can be measured with higher accuracy.
3. If neutrinos propagate through the core with a larger matter density, the effect of NSI in matter will be greater. As a result, the matter density, which can reach 11 g/cm³, makes this configuration special and promising for the measurement of $\epsilon_{\alpha\beta}$.
4. It is necessary to mention that though the statistics is lower as the baseline is much longer, this drawback can be compensated by the million-ton detector as PINGU.

This paper is arranged as follows. We will firstly demonstrate the neutrino oscillation probability with NSI matter effects, before presenting the simulation details. In the following, we will show the constraints on $\epsilon_{\alpha\beta}$ and constraint contours between any two of NSI parameters for the CERN-PINGU configuration. Moreover, we will discuss how this configuration can exclude the CP conserved scenario once the phase of $\epsilon_{\alpha\beta}$ is non-zero ($\alpha \neq \beta$). Finally, we will summarize our results, and provide our conclusion.

II. NEUTRINO OSCILLATION PHYSICS WITH NSIS

In this section, we briefly introduce how neutrino oscillation probabilities are modified by NSIs in matter. These new interactions are neutral-current-like interactions $\nu_\alpha + f \rightarrow \nu_\beta + f$, and can be described by the operator, [21, 45, 46],:

$$\mathcal{L}_{\text{NSI}} = -2\sqrt{2}G_F\epsilon_{\alpha\beta}^f (\bar{\nu}_\alpha\gamma^\mu P_L\nu_\beta) (\bar{f}\gamma_\mu P_C f') \quad (1)$$

where G_F is the Fermi constant. We note that the total size of NSI matter effects is the sum of those for NSIs with electrons, neutrons and protons: $\epsilon_{\alpha\beta} \equiv \epsilon_{\alpha\beta}^e + \epsilon_{\alpha\beta}^n + \epsilon_{\alpha\beta}^p$.

Neutrino oscillations are governed by coherent evolution of quantum states

$$i \frac{d}{dt} \begin{bmatrix} \nu_e \\ \nu_\mu \\ \nu_\tau \end{bmatrix} = H \begin{bmatrix} \nu_e \\ \nu_\mu \\ \nu_\tau \end{bmatrix}. \quad (2)$$

Explicitly, the evolution of the neutrino flavor state is determined by the Hamiltonian:

$$\begin{aligned} H_\nu &= H_{\text{vac}} + H_{\text{mat}} && \text{for } \nu, \\ H_{\bar{\nu}} &= [H_{\text{vac}} - H_{\text{mat}}]^* && \text{for } \bar{\nu}, \end{aligned} \quad (3)$$

where H_{vac} is the Hamiltonian in vacuum. H_{mat} corresponds to the matter, and is written by

$$H_{\text{mat}} = \sqrt{2}G_F N_e \begin{bmatrix} 1 + \epsilon_{ee} & \epsilon_{e\mu} & \epsilon_{e\tau} \\ \epsilon_{e\mu}^* & \epsilon_{\mu\mu} & \epsilon_{\mu\tau} \\ \epsilon_{e\tau}^* & \epsilon_{\mu\tau}^* & \epsilon_{\tau\tau} \end{bmatrix} \quad (4)$$

where N_e is the number density of electron. The constant term $\sqrt{2}G_F N_e$ in the ee component refers to the standard matter effect [21]. It is obvious in Eqs. (2) and (4) that one of the diagonal terms can be absorbed by an overall phase in neutrino states. Therefore, we define $\tilde{\epsilon}_{ee} \equiv \epsilon_{ee} - \epsilon_{\tau\tau}$ and $\tilde{\epsilon}_{\mu\mu} \equiv \epsilon_{\mu\mu} - \epsilon_{\tau\tau}$ without a loss of generality.

A. Analytical approximation

The main probabilities for the CERN-PINGU configuration to measure the effect of NSIs are via $P(\nu_\mu \rightarrow \nu_\mu)$ and $P(\nu_\mu \rightarrow \nu_e)$ and their CP-conjugate channels, because of the difficulty of the ν_τ and $\bar{\nu}_\tau$ detection. Taking $\frac{\Delta m_{21}^2}{\Delta m_{31}^2} \sim |\epsilon_{\alpha\beta}| \sim s_{13}^2$ as the first order of perturbation ξ , the approximation equations for the probability,

$$\begin{aligned} P(\nu_\mu \rightarrow \nu_\mu) &= P_0(\nu_\mu \rightarrow \nu_\mu) + \delta P_{\text{NSI}}(\nu_\mu \rightarrow \nu_\mu) \\ &= P_0(\nu_\mu \rightarrow \nu_\mu) - A\epsilon_{\mu\tau} \cos \phi_{\mu\tau} \\ &\quad \times \left(\sin^3 2\theta_{23} \frac{L}{2E} \sin 2\Delta_{31} \right. \\ &\quad \left. + 4 \sin 2\theta_{23} \cos^2 2\theta_{23} \frac{1}{\Delta m_{31}^2} \sin^2 \Delta_{31} \right) \\ &\quad + A\tilde{\epsilon}_{\mu\mu} c_{23}^2 s_{23}^2 (c_{23}^2 - s_{23}^2) \\ &\quad \times \left(\frac{L}{E} \sin 2\Delta_{31} - \frac{8}{\Delta m_{31}^2} \sin^2 \Delta_{31} \right) \\ &\quad + \mathcal{O}(\xi^2), \end{aligned} \quad (5)$$

B. Probabilities by numerical calculations

$$\begin{aligned}
P(\nu_\mu \rightarrow \nu_e) &= P_0(\nu_\mu \rightarrow \nu_e) + \delta P_{\text{NSI}}(\nu_\mu \rightarrow \nu_e) \\
&= P_0(\nu_\mu \rightarrow \nu_e) + 8s_{13}|\epsilon_{e\mu}|s_{23} \frac{\Delta m_{31}^2}{\Delta m_{31}^2 - A} \sin \Delta_{31}^A \\
&\times \left(s_{23}^2 \frac{A}{\Delta m_{31}^2 - A} \cos(\delta + \phi_{e\mu}) \sin \Delta_{31}^A \right. \\
&\left. + c_{23}^2 \sin \frac{AL}{4E} \cos(\delta + \phi_{e\mu} - \Delta_{31}) \right) \\
&+ 8s_{13}|\epsilon_{e\tau}|c_{23}s_{23}^2 \frac{\Delta m_{31}^2}{\Delta m_{31}^2 - A} \sin \Delta_{31}^A \\
&\times \left(\frac{A}{\Delta m_{31}^2 - A} \cos(\delta + \phi_{e\tau}) \sin \Delta_{31}^A \right. \\
&\left. - \sin \frac{AL}{4E} \cos(\delta + \phi_{e\tau} - \Delta_{31}) \right) \\
&+ \mathcal{O}(\xi^2), \tag{6}
\end{aligned}$$

where $P_0(\nu_\mu \rightarrow \nu_\mu)$ and $P_0(\nu_\mu \rightarrow \nu_e)$ are the probability for $\nu_\mu \rightarrow \nu_\mu$ and $\nu_\mu \rightarrow \nu_e$ channels without NSIs, respectively. And the notations Δ_{31} and Δ_{31}^A are defined as

$$\Delta_{31} \equiv \frac{\Delta m_{31}^2 L}{4E}, \text{ and } \Delta_{31}^A \equiv \frac{\Delta m_{31}^2 - A}{4E} \times L, \tag{7}$$

with $A \equiv 2\sqrt{2}G_F N_e E$. For antineutrino modes, the factors A and δ are replaced by $-A$ and $-\delta$, respectively. These equations are consistent with Ref. [47, 48]. The impact of NSIs is proportional to A . As a result, the increase of matter density enhances the measurement capacity of NSIs. In the configuration of CERN-PINGU, the matter density can reach up to 11 g/cm³, which is roughly three-time larger than the average matter density for DUNE (~ 3 g/cm³). Moreover, we notice that in $P(\nu_\mu \rightarrow \nu_\mu)$, one term for $\epsilon_{\mu\tau}$ and $\tilde{\epsilon}_{\mu\mu}$ are proportional to L , of which for the CERN-PINGU configuration is about nine-time longer than the baseline for DUNE 1300 km. We can expect the larger improvement in the measurement for these two NSI parameters from DUNE by the CERN-PINGU configuration. The same dependence on L is also seen for $\epsilon_{e\mu}$ and $\epsilon_{e\tau}$ in the appearance channel. However, they are higher order terms than $\tilde{\epsilon}_{\mu\mu}$ and $\epsilon_{\mu\tau}$.

The impact of $\phi_{e\mu}$ or $\phi_{e\tau}$ on $P(\nu_\mu \rightarrow \nu_e)$ depends on the value of δ and Δ_{31} . This dependence is not seen for $\phi_{\mu\tau}$ in $P(\nu_\mu \rightarrow \nu_\mu)$. As a result, the impact of δ and Δ_{31}^2 is larger in the measurement of $\phi_{e\mu}$ or $\phi_{e\tau}$. Also, $\epsilon_{e\mu}$ and $\epsilon_{e\tau}$ are the higher order than $\epsilon_{\mu\tau}$. Therefore, we can expect it is easier to detect the CP violation by $\phi_{\mu\tau}$, and even measure its size.

To sum up, we expect that the NSI measurement by the CERN-PINGU configuration can be better than what DUNE can achieve, because of the larger matter density. Though the matter density for this configuration is not overwhelmingly larger than that for DUNE. But the nine-time longer baseline can largely improve the measurement for $\epsilon_{e\tau}$ and $\tilde{\epsilon}_{\mu\mu}$ by the disappearance channels.

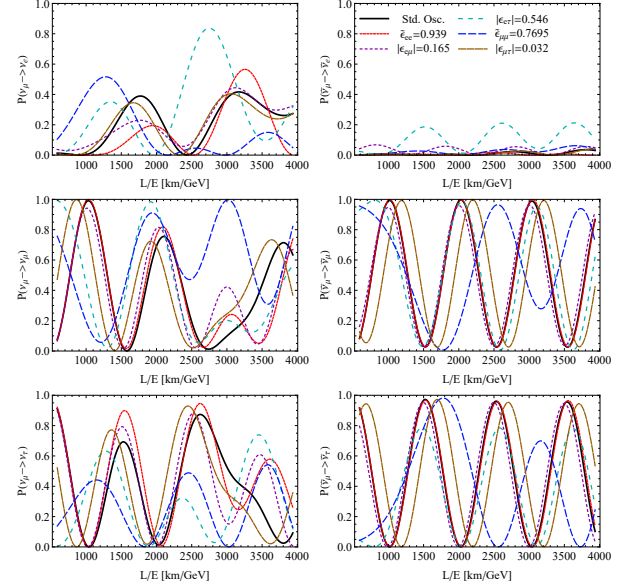


Figure 1. The neutrino oscillation probabilities $P(\nu_\mu \rightarrow \nu_e)$ (upper-left), $P(\bar{\nu}_\mu \rightarrow \bar{\nu}_e)$ (upper-right), $P(\nu_\mu \rightarrow \nu_\mu)$ (central-left), $P(\bar{\nu}_\mu \rightarrow \bar{\nu}_\mu)$ (central-right), $P(\nu_\mu \rightarrow \nu_\tau)$ (lower-left), and $P(\bar{\nu}_\mu \rightarrow \bar{\nu}_\tau)$ (lower-right) in the case with standard matter effects and in the case with nonzero $\epsilon_{\alpha\beta}$. The probabilities are shown as functions of L/E [km/GeV] in the range of $3 < E/\text{GeV} < 20$ with the baseline of 11810 km. The values are used according to the 1σ uncertainty of the current global fit result [14]. All phases are set to be 0.

Fig. 1 shows probabilities in each of channels in the case only including standard matter effects, and for those with a non-zero $\epsilon_{\alpha\beta}$, of which the value is used according to the 1σ bound of the current global fit result [14]. These probabilities are shown as functions of L/E [km/GeV] in the range of neutrino energy (3 GeV - 20 GeV) with the baseline of 11810 km. We obtain that the behavior of probabilities for non-zero $\tilde{\epsilon}_{\mu\mu}$ or $|\epsilon_{\mu\tau}|$ in some channels is very different from that without NSI matter effects. For example, when $L/E = 2700$ [km/GeV], $P(\nu_\mu \rightarrow \nu_e)$ is about 0.8 in the case with non-zero $|\epsilon_{\mu\tau}|$, while it is around 0.2 for the standard case. We also see that the probability of the $\bar{\nu}_\mu$ disappearance channel approaches the maximum at $L/E = 2500$ [km/GeV] in the non-zero case of $\tilde{\epsilon}_{\mu\mu}$, while this probability is around zero in the framework of standard neutrino oscillations.

The probabilities with possible values of $\phi_{\alpha\beta}$ are shown in Fig. 2. We vary each phase $\phi_{\alpha\beta}$ from -180° to 180° , and fix the value of $|\epsilon_{\alpha\beta}|$ at 0.05. Two probabilities $P(\nu_\mu \rightarrow \nu_e)$ and $P(\nu_\mu \rightarrow \nu_\mu)$ are shown, because events in the other channels are less than these two. We find the variation of the probability is the most dramatic for $\phi_{\mu\tau}$. What follows is that for $\phi_{e\tau}$, while the smallest one is for $\phi_{e\mu}$. We see the same result in the other channels.

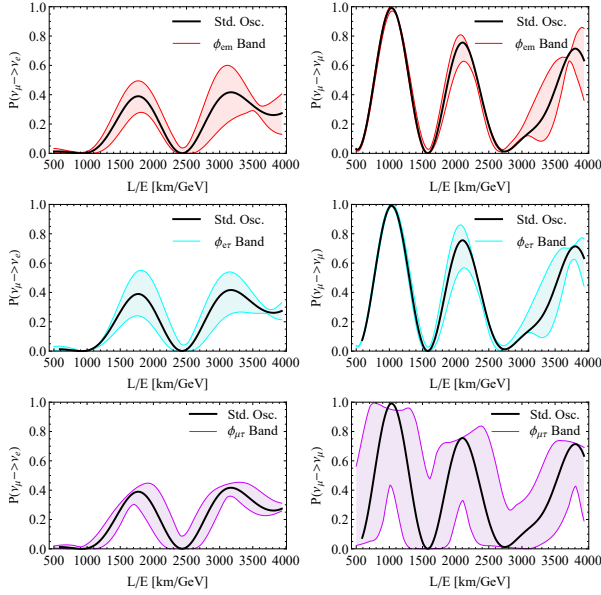


Figure 2. The neutrino oscillation probabilities $P(\nu_\mu \rightarrow \nu_e)$ (left panels), $P(\nu_\mu \rightarrow \nu_\mu)$ (right panels) for phases $\phi_{e\mu}$ (pink), $\phi_{e\tau}$ (light blue) and $\phi_{\mu\tau}$ (light-magenta) varying over $(-180^\circ, 180^\circ]$. For the band with non-zero $\phi_{\alpha\beta}$, the absolute value $|\epsilon_{\alpha\beta}|$ is fixed at 0.05. The probabilities are shown as functions of L/E [km/GeV] in the range of $3 < E/\text{GeV} < 20$ with the baseline of 11810 km.

C. The θ_{23} - $\tilde{\epsilon}_{\mu\mu}$ degeneracy

There is a degeneracy between θ_{23} and $\tilde{\epsilon}_{\mu\mu}$. This degeneracy can be easier to be understood by further taking $\delta\theta_{23} \equiv \theta_{23} - 45^\circ$ as a perturbation at the first order $\mathcal{O}(\xi)$. For the disappearance channel,

$$\begin{aligned}
 P(\nu_\mu \rightarrow \nu_\mu) = & P_0(\nu_\mu \rightarrow \nu_\mu) - |\epsilon_{\mu\tau}| \cos \phi_{\mu\tau} \frac{AL}{2E} \sin 2\Delta_{31} \\
 & - 2\delta\theta_{23} \tilde{\epsilon}_{\mu\mu} A \times \left(\frac{L}{E} \sin 2\Delta_{31} \right. \\
 & \left. - \frac{8}{\Delta m_{31}^2} \sin^2 \Delta_{31} \right) + \mathcal{O}(\xi^2) \quad (8)
 \end{aligned}$$

This is obvious that there is a degeneracy between $\delta\theta_{23}$ and $\tilde{\epsilon}_{\mu\mu}$. In our work, $\delta\theta_{23} \sim 0.08$ for the true value $\theta_{23} = 49.7^\circ$. This degeneracy has also been studied in Ref. [25, 48–51].

The degeneracy between $\tilde{\epsilon}_{ee}$ and $\epsilon_{\tau\tau}$ that is from the higher order terms has been also studied in Ref. [25, 52].

III. SIMULATION DETAILS

We adopt General Long Baseline Experiment Simulator [53, 54] with the PINGU simulation package.

For the production, we assume μ decays driving the

Table I. Disappearance and appearance channels considered in this experiment.

Disappearance channels		appearance channels	
$\nu_\mu \rightarrow \nu_\mu$		$\nu_\mu \rightarrow \nu_e$	
		$\bar{\nu}_\mu \rightarrow \bar{\nu}_e$	
$\bar{\nu}_\mu \rightarrow \bar{\nu}_\mu$		$\nu_\mu \rightarrow \nu_\tau$	
		$\bar{\nu}_\mu \rightarrow \bar{\nu}_\tau$	

production of neutrinos:

$$\pi^- \rightarrow \mu^- + \nu_\mu, \quad (9)$$

$$\pi^+ \rightarrow \mu^+ + \bar{\nu}_\mu. \quad (10)$$

We set the run time of 5 years for neutrino and antineutrino modes (total run time is 10 years) with 1×10^{20} protons on target (POTs) per year. The energy of protons is assumed 120 GeV and the power is 708 kW.

To include NSI matter effects, we adopt the GLoBES extension package mentioned in Refs. [55–58]. We adopt the PREM onion shell model of the earth for the matter density profile [59, 60], which is shown in Appendix A. The matter density can reach 11 g/cm^3 .

All oscillation channels are listed in Table I. We consider the intrinsic ν_e and $\bar{\nu}_e$ backgrounds in the beam and the atmospheric neutrino backgrounds. We note that Water Cherenkov neutrino detector cannot make a distinction between neutrinos and antineutrinos. Therefore, for the electron-flavor channels, we analyse the combination of ν_e and $\bar{\nu}_e$ spectra. Because of the difficulty of ν_τ and $\bar{\nu}_\tau$ detection, we adopt a relative conserved assumption for detection efficiency for ν_τ and $\bar{\nu}_\tau$.

The expected spectra are shown in Fig. 3. We compare the case with standard matter effects to that in vacuum, for demonstrating the advantage of the CERN-PINGU configuration to collect matter effects through such a long baseline 11810 km. Assumed the normal mass ordering, events are much less in the $\bar{\nu}$ mode. We see that matter effects make great impacts on the spectra in the ν_e appearance and ν_μ and $\bar{\nu}_\mu$ disappearance channels for the lower neutrino energy.

Values used for oscillation and NSI parameters through this paper are listed in Table II. These values are taken from current global-fit results [2, 14]. The normal mass ordering is assumed. We neglect NSIs at the source and detector, and marginalise over all parameters, including standard oscillation parameters, the matter density and eight parameters for NSIs in matter ($\epsilon_{\tau\tau}$ is subtracted by an overall phase of neutrino states) unless we showed them in the plot.

IV. RESULTS

In this section, our simulation results will be presented. In Sec. IV A, we will firstly show the expected constraints on $\epsilon_{\alpha\beta}$ for the CERN-PINGU configuration. In the following section, we will discuss the sensitivity of CPV in

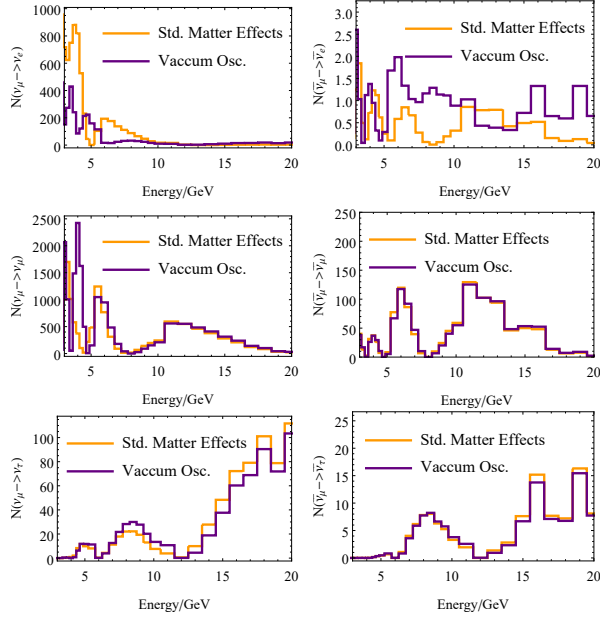


Figure 3. The spectra for $P(\nu_\mu \rightarrow \nu_e)$ (upper-left), $P(\bar{\nu}_\mu \rightarrow \bar{\nu}_e)$ (upper-right), $P(\nu_\mu \rightarrow \nu_\mu)$ (central-left), $P(\bar{\nu}_\mu \rightarrow \bar{\nu}_\mu)$ (central-right), $P(\nu_\mu \rightarrow \nu_\tau)$ (lower-left), and $P(\bar{\nu}_\mu \rightarrow \bar{\nu}_\tau)$ (lower-right) with (purple) and without (orange) the standard matter effects. The ν_τ and $\bar{\nu}_\tau$ spectra shown here are optimistic without considering the detection difficulty.

Table II. The central value and the width of the prior for standard neutrino oscillation and NSI parameters used throughout our simulation. We note that the central values are as same as the true values, except for the case in which the true values are specified. These values are used according to current global fit results [2, 14].

parameter	true/central value	1σ width
$\theta_{12}/^\circ$	33.82	2%
$\theta_{13}/^\circ$	8.61	2%
$\theta_{23}/^\circ$	49.7	2%
$\Delta m_{21}^2/10^{-5}\text{eV}$	7.38	2%
$\Delta m_{31}^2/10^{-3}\text{eV}$	2.525	1%
$\delta_{\text{CP}}/^\circ$	217	10%
$\tilde{\epsilon}_{ee}$	0	0.939
$\tilde{\epsilon}_{\mu\mu}$	0	0.7695
$ \epsilon_{e\mu} $	0	0.165
$ \epsilon_{e\tau} $	0	0.546
$ \epsilon_{\mu\tau} $	0	0.0315
$\phi_{e\mu}$	0	no restriction
$\phi_{e\tau}$	0	no restriction
$\phi_{\mu\tau}$	0	no restriction

NSIs. In more details, what will be studied further is how much the hypothesis $\phi_{\alpha\beta} = 0$ and π can be excluded by this configuration, once CP is violated because of non-zero of $\phi_{\alpha\beta}$.

A. Constraints on NSI parameters

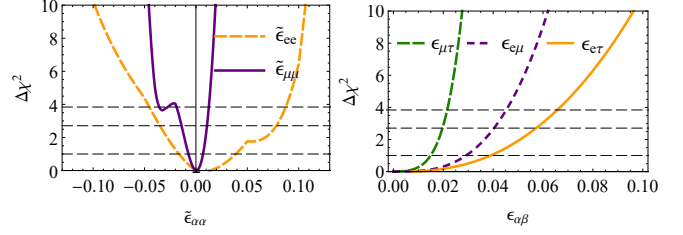


Figure 4. $\Delta\chi^2$ value against $\tilde{\epsilon}_{\alpha\alpha}$ (left) and $|\epsilon_{\alpha\beta}|$ (right). The three dashed lines represent the values at 68%, 90% and 95% C.L. The central values and priors of neutrino mixing parameters are taken from Table II.

The $\Delta\chi^2$ values against to each NSI parameter are shown in Fig. 4. The size of the 1σ uncertainty for $\tilde{\epsilon}_{ee}$ is about $-0.03 < \epsilon_{\mu\mu} < 0.01$. We find out a degeneracy around $\tilde{\epsilon}_{\mu\mu} = -0.035$ with $\Delta\chi^2 \gtrsim 4$. For the off-diagonal terms, bounds at 1σ C.L. are at $|\epsilon_{e\mu}| \sim 0.03$, $|\epsilon_{e\tau}| \sim 0.04$, and $|\epsilon_{\mu\tau}| \sim 0.015$, respectively. We reach the conclusion that constraints on $\tilde{\epsilon}_{\mu\mu}$ and $|\epsilon_{\mu\tau}|$ are better than the others, which is consistent with the conclusion of Secs. II A and II B. We review the 1σ uncertainties in the current global fit result, which are shown in Table II. We see the weak constraint at 1σ C.L. on the diagonal terms $\tilde{\epsilon}_{ee}$ and $\tilde{\epsilon}_{\mu\mu}$, whose sizes are almost $\mathcal{O}(1)$. As for the off-diagonal terms, we have better understandings in the global fit. The size of 1σ uncertainty is smaller than 0.1, especially the 1σ uncertainty for $\epsilon_{\mu\tau}$ is 0.0315. We find that the CERN-PINGU configuration can improve sensitivities of NSIs at 1σ C.L. by at least 50% of the current global fit result. As the uncertainty for $\tilde{\epsilon}_{ee}$ is greatly improved, we have the interest on the exclusion ability of the LMA-dark solution. Though the result is not shown here, we have checked that the LMA-dark solution can be excluded by more than 5σ C.L., without any prior for θ_{12} and ϵ_{ee} .

In Fig. 5, we show the allowed region at 68%, 90%, 95% confidence level (C.L.) on the projected plane spanned by two of NSI parameters. Though we do not see strong correlations in these results, a degeneracy for $\tilde{\epsilon}_{\mu\mu} \sim -0.035$ can be seen for contours of 90% and 95% C.L. As mentioned in Sec. II C, this degeneracy is caused with the mixing angle θ_{23} . Mentioned in Ref. [25], this degeneracy can be removed by including T2HK data. Obviously, the degeneracy between $\tilde{\epsilon}_{ee}$ and $\epsilon_{\tau e}$ and the one around $\tilde{\epsilon}_{\mu\mu} = 0.5$ for DUNE, are excluded.

In Fig. 6, we present allowed regions on the plane spanned by the absolute value $|\epsilon_{\alpha\beta}|$ and the phase $\phi_{\alpha\beta}$ for off-diagonal elements $\epsilon_{e\mu}$, $\epsilon_{e\tau}$, and $\epsilon_{\mu\tau}$ at 68%, 90% and 95% C.L.. We see a strong correlation between the absolute value and the phase in these three panels. For the hypothesis with $\phi_{\alpha\beta}$ near $\pm 90^\circ$, the bound on the absolute value $|\epsilon_{\alpha\beta}|$ is the worst. This behavior also applies to all off-diagonal elements. $\epsilon_{\alpha\beta}$ will be improved

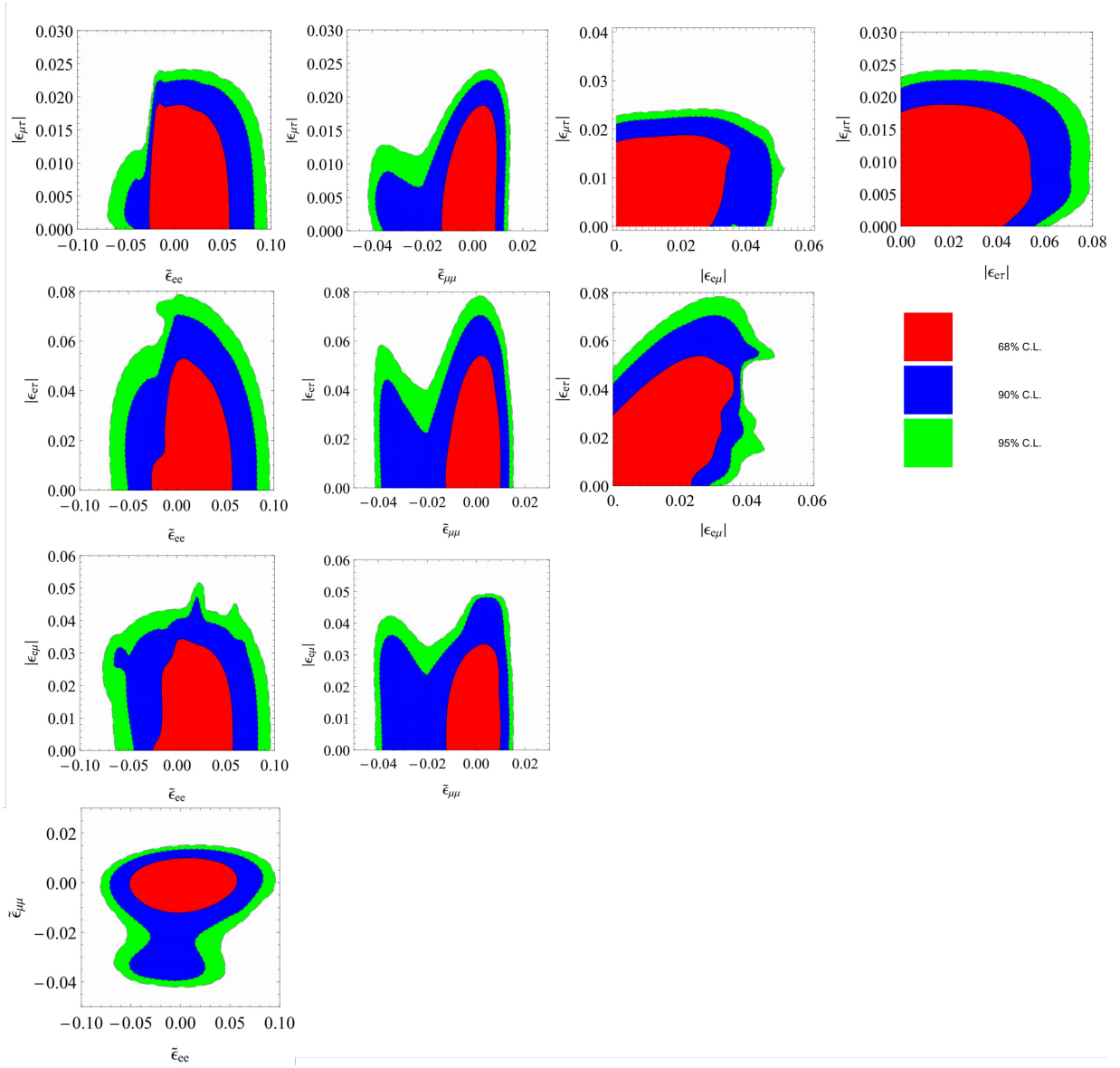


Figure 5. The allowed regions on the plane spanned by two of NSI parameters. The central values and priors are taken from Table II. All parameters are marginalized except those shown in each panel.

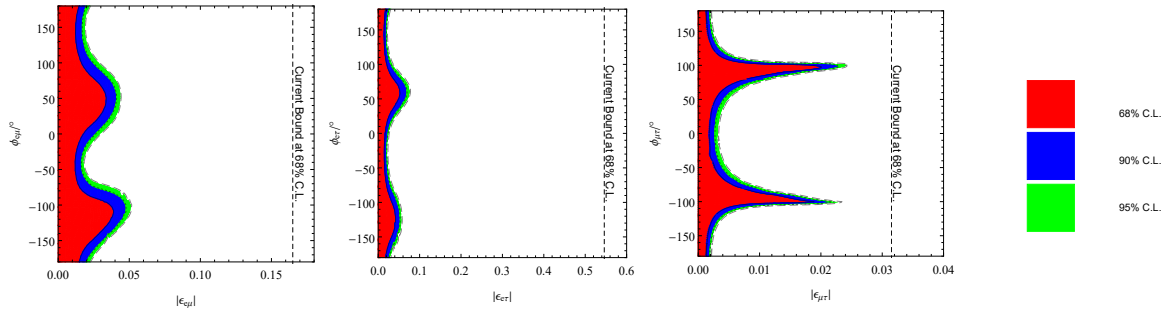


Figure 6. The allowed region on the plane spanned by the absolute value $|\epsilon_{\alpha\beta}|$ and the phase $\phi_{\alpha\beta}$ for off-diagonal elements $\epsilon_{e\mu}$ (left), $\epsilon_{e\tau}$ (middle), and $\epsilon_{\mu\tau}$ (right) at 68% (red), 90% (blue) and 95% (green) C.L.. All parameters are marginalized over except those shown in each panel.

by more than an order of magnitude. Compared with sensitivities of NSIs at DUNE, our proposal will improve

results by at least a factor of three. Of course, the phase of NSI parameters will play an important role here.

B. CP violations of NSI

We further discuss how the CERN-PINGU configuration can exclude the CP-conserved scenario where $\phi_{\alpha\beta}$ is neither 0 nor 180° . We study the CPV sensitivity, which is defined

$$\Delta\chi_{CP}^2(\phi_{\alpha\beta}^{true}) \equiv \min\{\Delta\chi^2(\phi_{\alpha\beta} = 0), \Delta\chi^2(\phi_{\alpha\beta} = \pi)\}, \quad (11)$$

where $\phi_{\alpha\beta}^{true}$ is the true value for $\phi_{\alpha\beta}$, and $\Delta\chi^2(\phi_{\alpha\beta} = 0)$ and $\Delta\chi^2(\phi_{\alpha\beta} = 180^\circ)$ are the $\Delta\chi^2$ value for the hypothesis $\phi_{\alpha\beta} = 0$ and 180° respectively. This definition is same as how we study the sensitivity of CP violation where δ_{CP} is not 0 or 180° .

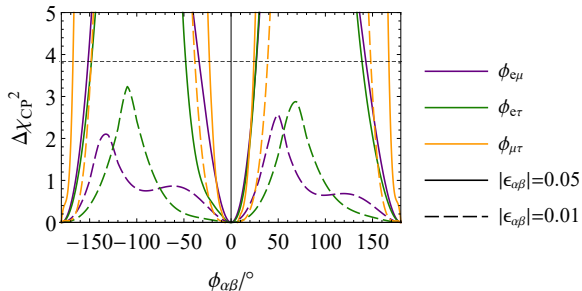


Figure 7. The $\Delta\chi_{CP}^2$ value against to the phase for the $e\mu$ (purple), $e\tau$ (green), and $\mu\tau$ (orange) components. For the studied component, the true absolute value is 0.05 (solid) and 0.01 (dashed), while the other NSIs are switched off.

In Fig. 7, we study the value of $\Delta\chi_{CP}^2$ for three phases: $\phi_{e\mu}$, $\phi_{e\tau}$ and $\phi_{\mu\tau}$ in the range between -180° and 180° . For $\Delta\chi_{CP}^2(\phi_{\alpha\beta})$, we fix the absolute value of the other two off-diagonal terms at 0, as we focus on the CP violation by one specific $\phi_{\alpha\beta}$. Studying $\Delta\chi_{CP}^2(\phi_{\alpha\beta})$ values, we set the true value of $|\epsilon_{\alpha\beta}|$ to be 0.05 (solid) and 0.01 (dashed). We focus on the case with the absolute value fixed at 0.05. We see that the CPV sensitivity for $\phi_{\mu\tau}$ is the best. In about 81% of possible $\phi_{\mu\tau}$ this configuration can exclude the CP-conserved scenario with the significance better than 95% C.L.. $\Delta\chi_{CP}^2(\phi_{e\tau})$ is slightly better than $\Delta\chi_{CP}^2(\phi_{e\mu})$. For $\Delta\chi_{CP}^2(\phi_{e\tau})$ ($\Delta\chi_{CP}^2(\phi_{e\mu})$) larger than the value for 95% C.L., it covers 75% (63%) of all possible phases. With the absolute value of 0.01, the sensitivity is worse, especially for $\phi_{e\mu}$ and $\phi_{e\tau}$, of which $\Delta\chi_{CP}^2$ is smaller than 3.5. For $\epsilon_{\mu\tau}$, phases with the sensitivity larger than 90% C.L. cover about 75% of all possible phases. We note that the result shown in Fig. 7 is consistent with what we see in Fig. 2. Our simulation result is based on the assumption that we focus on one specific off-diagonal element. Though not shown here, we find that once we also marginalize over absolute values and phases of the other off-diagonal terms, the sensitivity is much worse.

C. Comparison with the other experiments

In Table III, we compare the CERN-PINGU configuration with the other future accelerator neutrino oscillation experiments, DUNE, T2HK, and the Protvino-ORCA experiment (P2O), with the simulation details about these configuration. For all of them, we use the PREM onion shell model of the earth for the matter density [59, 60], and include the prior that presents the constraint with the global and COHERENCE [14]. Taking the same fluxes, effective masses, our ν -mode simulation for P2O reproduces the event spectra in [62, 63]. However, because the spectra for $\bar{\nu}$ are not shown in this reference, we use the same detection efficiency for $\bar{\nu}$ same as those for ν . The other assumption for detection is used the same as what we use for PINGU. We find that the CERN-PINGU configuration performs the best among all, and that T2HK is the worst one to measure NSI parameters. The constraints of the CERN-PINGU configuration is smaller than DUNE by at least a factor of 0.1. We need to point it out that for this result, DUNE requests 0 more POTs than that for the CERN-PINGU configuration, by a factor of ~ 10 . The physics capability of P2O to measure NSI parameters, is the closet one to the CERN-PINGU configuration. The measurements of $|\epsilon_{e\mu}|$ and $|\epsilon_{e\tau}|$ for the CERN-PINGU configuration are slightly better than those for P2O. The constraint of $|\epsilon_{\mu\tau}|$ by the CERN-PINGU configuration can be 20% of the result by P2O. Finally, the measurement of the diagonal terms for the CERN-PINGU configuration can be improved by one order of magnitude, than that for P2O.

V. CONCLUSION

With the interest on the planet-scale neutrino oscillations, we have considered the configuration that neutrinos are generated at CERN, and detected in the PINGU detector (CERN-PINGU), as an extended study of Ref. [10]. We have analyzed how such a configuration can measure the size of non-standard interactions (NSIs) in matter. Three advantages of this configuration are as follows: (1) the energy range 3 GeV-20 GeV enhancing effects of NSIs, (2) the 11810-km baseline cumulating these effects, and (3) the high matter density 11 g/cm³ making the impact of NSIs on neutrino oscillations more significant.

We have adopted the GLOBES library with an extension package to simulate the CERN-PINGU configuration for the neutrino oscillation with NSI matter effects. We have studied the predicted uncertainty of NSI parameters $\epsilon_{\alpha\beta}$. We have found that this configuration measures $\tilde{\epsilon}_{\mu\mu} \equiv \epsilon_{\mu\mu} - \epsilon_{\tau\tau}$ and $|\epsilon_{\mu\tau}|$ better than the others. Most of degeneracy problems for DUNE on $\epsilon_{\alpha\beta}$ measurements are resolved, except the one around $\tilde{\epsilon}_{\mu\mu} \sim -0.035$. We have investigated strong correlations between the absolute value and the phase for all off-diagonal terms, which can also be seen in the recent work with regards to

Table III. The 1σ allowed range of $\tilde{\epsilon}_{ee}$, $\tilde{\epsilon}_{\mu\mu}$, $|\epsilon_{e\mu}|$, $|\epsilon_{e\tau}|$, and $|\epsilon_{\mu\tau}|$ for the CERN-PINGU configuration, DUNE, T2HK and P2O experiments. We also present the simulation details for each experiments.

parameter	CERN-PINGU	DUNE [23]	T2HK [61]	P2O [62, 63]
$\tilde{\epsilon}_{ee}$	$[-0.0163, 0.0390]$	$[-1.0025, 1.146]$	$[-2.2069, 2.2934]$	$[-0.1944, 0.1633]$
$\tilde{\epsilon}_{\mu\mu}$	$[-0.0075, 0.0067]$	$[-0.0753, 0.0769]$	$[-0.2530, 0.2588]$	$[-0.0409, 0.0328]$
$ \epsilon_{e\mu} $	$[0, 0.0291]$	$[0, 0.1018]$	$[0.4062]$	$[0, 0.0346]$
$ \epsilon_{e\tau} $	$[0, 0.0389]$	$[0, 0.1938]$	$[0, 0.2624]$	$[0, 0.039]$
$ \epsilon_{\mu\tau} $	$[0, 0.0148]$	$[0, 0.2012]$	$[0, 0.9136]$	$[0, 0.0719]$
POTs	10×10^{20}	8.82×10^{21}	2.7×10^{22}	2.4×10^{20}
Energy range [GeV]	3-20	0.5-8	0.1-1.2	2-12
Baseline [km]	11810	1300	295	2595
Target material	ice	liquid argon	pure water	sea water
Detector size [kton]	$\mathcal{O}(10^3)$	40	186	$\mathcal{O}(10^3)$

NSI-parameter measurements for DUNE. As phases $\phi_{\alpha\beta}$ play important roles, we have extended our study on the sensitivity of CP violation in NSIs. We have found that with the absolute value of 0.05 the sensitivity can be better than 95% C.L. in the CERN - PINGU configuration, which shows this configuration can be used to measure the CP violation caused by NSIs. Compared to other experiments, DUNE, T2HK, and P2O, we find that the CERN-PINGU configuration can significantly improve the constraints of NSI parameters, except the measurements of $\epsilon_{e\mu}$ and $\epsilon_{e\tau}$, for which the CERN-PINGU configuration performs slightly better than P2O.

This study should not be limited at the CERN-PINGU configuration. Our conclusion on the improvement of $\epsilon_{\alpha\beta}$ measurements could be applied for any experiments with the neutrino source or detector that satisfies three requirements: the proper energy range, a planet-scale baseline, and the high matter density. As PINGU is under consideration, we can put more focus on looking for possible sources, such as accelerator neutrinos produced by future proton drivers as super proton-proton collider (SPPC) [64], and the point source of astrophysical neutrinos [65].

ACKNOWLEDGMENTS

This work is supported in part by the grant National Natural Science Foundation of China under Grant No. 11505301 and No. 1188124024. JT appreciate ICTP's hospitality and discussions during the workshop

PANE2018. Wei-Jie Feng and Yi-Xing Zhou are supported in part by Innovation Training Program for bachelor students at School of Physics in SYSU.

Appendix A: The matter density profile for CERN-PINGU

Fig. 8, the matter density profile used in GLoBES simulation for the CERN-PINGU configuration. The x-axis is the distance from the source toward the detector. As

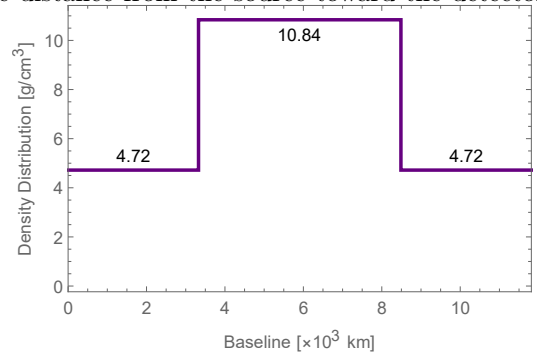


Figure 8. The matter density profile used in GLoBES simulation for the CERN-PINGU configuration. The x-axis is the distance from the source toward the detector.

we can see, the density can achieve up to 10.84 g/cm³ from the oscillation distance 3500 km to 8000 km.

-
- [1] Takaaki Kajita. Atmospheric neutrino results from Super-Kamiokande and Kamiokande: Evidence for neutrino(mu) oscillations. *Nucl. Phys. Proc. Suppl.*, 77:123–132, 1999. [,123(1998)].
- [2] Ivan Esteban, M. C. Gonzalez-Garcia, Alvaro Hernandez-Cabezudo, Michele Maltoni, and Thomas Schwetz. Global analysis of three-flavour neutrino oscillations: synergies and tensions in the determination of θ_{23} , δ_{CP} ,

- and the mass ordering. *JHEP*, 01:106, 2019.
- [3] P. F. De Salas, S. Gariazzo, O. Mena, C. A. Ternes, and M. Tortola. Neutrino Mass Ordering from Oscillations and Beyond: 2018 Status and Future Prospects. *Front. Astron. Space Sci.*, 5:36, 2018.
- [4] F. Capozzi, E. Lisi, A. Marrone, and A. Palazzo. Current unknowns in the three neutrino framework. *Prog. Part. Nucl. Phys.*, 102:48–72, 2018.

- [5] M. G. Aartsen et al. PINGU: A Vision for Neutrino and Particle Physics at the South Pole. *J. Phys.*, G44(5):054006, 2017.
- [6] Sandhya Choubey and Tommy Ohlsson. Bounds on non-standard neutrino interactions using pingu. *Physics Letters B*, 739:357–364, 2014.
- [7] Walter Winter. Neutrino mass hierarchy determination with icecube-pingu. *Physical Review D*, 88(1):013013, 2013.
- [8] PINGU Collaboration et al. Letter of intent: the precision icecube next generation upgrade (pingu). *arXiv preprint arXiv:1401.2046*, 2014.
- [9] D Jason Koskinen. Icecube-deepcore-pingu: Fundamental neutrino and dark matter physics at the south pole. *Modern Physics Letters A*, 26(39):2899–2915, 2011.
- [10] Jian Tang and Walter Winter. Requirements for a new detector at the south pole receiving an accelerator neutrino beam. *Journal of High Energy Physics*, 2012(2):28, Feb 2012.
- [11] Tommy Ohlsson. Status of non-standard neutrino interactions. *Rept. Prog. Phys.*, 76:044201, 2013.
- [12] O. G. Miranda and H. Nunokawa. Non standard neutrino interactions: current status and future prospects. *New J. Phys.*, 17(9):095002, 2015.
- [13] Y. Farzan and M. Tortola. Neutrino oscillations and Non-Standard Interactions. *Front.in Phys.*, 6:10, 2018.
- [14] Ivan Esteban, M. C. Gonzalez-Garcia, Michele Maltoni, Ivan Martinez-Soler, and Jordi Salvado. Updated Constraints on Non-Standard Interactions from Global Analysis of Oscillation Data. *JHEP*, 08:180, 2018.
- [15] P. S. Bhupal Dev et al. Neutrino Non-Standard Interactions: A Status Report. In *NTN Workshop on Neutrino Non-Standard Interactions St Louis, MO, USA, May 29-31, 2019*, 2019.
- [16] A. Acker, S. Pakvasa, and James T. Pantaleone. Decaying Dirac neutrinos. *Phys. Rev.*, D45:1–4, 1992.
- [17] Andy Acker and Sandip Pakvasa. Solar neutrino decay. *Phys. Lett.*, B320:320–322, 1994.
- [18] Jian Tang, Tse-Chun Wang, and Yibing Zhang. Invisible neutrino decays at the MOMENT experiment. *JHEP*, 04:004, 2019.
- [19] J. Schechter and J. W. F. Valle. Neutrino masses in $su(2) \otimes u(1)$ theories. *Phys. Rev. D*, 22:2227–2235, Nov 1980.
- [20] O. G. Miranda, Pedro Pasquini, M. Tortola, and J. W. F. Valle. Exploring the Potential of Short-Baseline Physics at Fermilab. *Phys. Rev.*, D97(9):095026, 2018.
- [21] Lincoln Wolfenstein. Neutrino oscillations in matter. *Physical Review D*, 17(9):2369, 1978.
- [22] M. M. Guzzo, A. Masiero, and S. T. Petcov. On the MSW effect with massless neutrinos and no mixing in the vacuum. *Phys. Lett.*, B260:154–160, 1991. [,369(1991)].
- [23] R. Acciarri et al. Long-Baseline Neutrino Facility (LBNF) and Deep Underground Neutrino Experiment (DUNE). 2015.
- [24] B. Abi et al. The DUNE Far Detector Interim Design Report Volume 1: Physics, Technology and Strategies. 2018.
- [25] Pilar Coloma. Non-Standard Interactions in propagation at the Deep Underground Neutrino Experiment. *JHEP*, 03:016, 2016.
- [26] Mehedi Masud, Animesh Chatterjee, and Poonam Mehta. Probing CP violation signal at DUNE in presence of non-standard neutrino interactions. *J. Phys.*, G43(9):095005, 2016.
- [27] Jiajun Liao, Danny Marfatia, and Kerry Whisnant. Degeneracies in long-baseline neutrino experiments from nonstandard interactions. *Phys. Rev.*, D93(9):093016, 2016.
- [28] Sanjib Kumar Agarwalla, Sabya Sachi Chatterjee, and Antonio Palazzo. Degeneracy between θ_{23} octant and neutrino non-standard interactions at DUNE. *Phys. Lett.*, B762:64–71, 2016.
- [29] Mehedi Masud and Poonam Mehta. Nonstandard interactions and resolving the ordering of neutrino masses at DUNE and other long baseline experiments. *Phys. Rev.*, D94(5):053007, 2016.
- [30] David V. Forero and Patrick Huber. Hints for leptonic CP violation or New Physics? *Phys. Rev. Lett.*, 117(3):031801, 2016.
- [31] Mehedi Masud and Poonam Mehta. Nonstandard interactions spoiling the CP violation sensitivity at DUNE and other long baseline experiments. *Phys. Rev.*, D94:013014, 2016.
- [32] Shao-Feng Ge and Alexei Yu. Smirnov. Non-standard interactions and the CP phase measurements in neutrino oscillations at low energies. *JHEP*, 10:138, 2016.
- [33] Katri Huitu, Timo J. Karkkainen, Jukka Maalampi, and Sampsa Vihonen. Constraining the nonstandard interaction parameters in long baseline neutrino experiments. *Phys. Rev.*, D93(5):053016, 2016.
- [34] Monojit Ghosh and Osamu Yasuda. Effect of systematics in the T2HK, T2HKK, and DUNE experiments. *Phys. Rev.*, D96(1):013001, 2017.
- [35] L. J. Flores, E. A. Garcé s, and O. G. Miranda. Exploring NSI degeneracies in long-baseline experiments. *Phys. Rev.*, D98(3):035030, 2018.
- [36] Mehedi Masud, Samiran Roy, and Poonam Mehta. Correlations and degeneracies among the NSI parameters with tunable beams at DUNE. *Phys. Rev.*, D99(11):115032, 2019.
- [37] Francesco Capozzi, Sabya Sachi Chatterjee, and Antonio Palazzo. Neutrino mass ordering obscured by non-standard interactions. 2019.
- [38] Anish Ghoshal, Alessio Giannetti, and Davide Meloni. On the Role of the ν_τ Appearance in DUNE in Constraining Standard Neutrino Physics and Beyond. 2019.
- [39] I. Girardi, D. Meloni, and S. T. Petcov. The Daya Bay and T2K results on $\sin^2 2\theta_{13}$ and Non-Standard Neutrino Interactions. *Nucl. Phys.*, B886:31–42, 2014.
- [40] Yasaman Farzan. A model for large non-standard interactions of neutrinos leading to the LMA-Dark solution. *Phys. Lett.*, B748:311–315, 2015.
- [41] Yasaman Farzan and Ian M. Shoemaker. Lepton Flavor Violating Non-Standard Interactions via Light Mediators. *JHEP*, 07:033, 2016.
- [42] Yasaman Farzan and Julian Heeck. Neutrinophilic non-standard interactions. *Phys. Rev.*, D94(5):053010, 2016.
- [43] David V. Forero and Wei-Chih Huang. Sizable NSI from the $SU(2)_L$ scalar doublet-singlet mixing and the implications in DUNE. *JHEP*, 03:018, 2017.
- [44] K. S. Babu, P. S. Bhupal Dev, Sudip Jana, and Anil Thapa. Non-Standard Interactions in Radiative Neutrino Mass Models. 2019.
- [45] Yuval Grossman. Non-standard neutrino interactions and neutrino oscillation experiments. *Physics Letters B*, 359(1):141 – 147, 1995.
- [46] Zurab Berezhiani and Anna Rossi. Limits on the non-standard interactions of neutrinos from $e^+ e^-$ colliders.

- Phys. Lett.*, B535:207–218, 2002.
- [47] TseChun Wang and Ye-Ling Zhou. Neutrino nonstandard interactions as a portal to test flavor symmetries. *Phys. Rev.*, D99(3):035039, 2019.
- [48] Takashi Kikuchi, Hisakazu Minakata, and Shoichi Uchinami. Perturbation Theory of Neutrino Oscillation with Nonstandard Neutrino Interactions. *JHEP*, 03:114, 2009.
- [49] P. Coloma, A. Donini, J. Lopez-Pavon, and H. Minakata. Non-Standard Interactions at a Neutrino Factory: Correlations and CP violation. *JHEP*, 08:036, 2011.
- [50] Alexander Friedland, Cecilia Lunardini, and Michele Maltoni. Atmospheric neutrinos as probes of neutrino-matter interactions. *Phys. Rev.*, D70:111301, 2004.
- [51] Alexander Friedland and Cecilia Lunardini. Two modes of searching for new neutrino interactions at MINOS. *Phys. Rev.*, D74:033012, 2006.
- [52] Mariano Esteves Chaves, Diego Rossi Gratieri, and Orlando Luis Goulart Peres. Improvements on perturbative oscillation formulas including non-standard neutrino Interactions. 2018.
- [53] P. Huber, M. Lindner, and W. Winter. Simulation of long-baseline neutrino oscillation experiments with globes: (general long baseline experiment simulator). *Computer Physics Communications*, 167(3):195 – 202, 2005.
- [54] Patrick Huber, Joachim Kopp, Manfred Lindner, Mark Rolinec, and Walter Winter. New features in the simulation of neutrino oscillation experiments with globes 3.0: (general long baseline experiment simulator). *Computer Physics Communications*, 177(5):432 – 438, 2007.
- [55] Joachim Kopp. Efficient numerical diagonalization of hermitian 3×3 matrices. *Int. J. Mod. Phys.*, C19:523–548, 2008.
- [56] Joachim Kopp, Manfred Lindner, and Toshihiko Ota. Discovery reach for nonstandard interactions in a neutrino factory. *Phys. Rev. D*, 76:013001, Jul 2007.
- [57] Joachim Kopp, Manfred Lindner, Toshihiko Ota, and Joe Sato. Nonstandard neutrino interactions in reactor and superbeam experiments. *Phys. Rev. D*, 77:013007, Jan 2008.
- [58] Jian Tang and Yibing Zhang. Study of nonstandard charged-current interactions at the moment experiment. *Phys. Rev. D*, 97:035018, Feb 2018.
- [59] F. D. Stacey. *Physics of the earth*. Wiley, 2nd edition, 1977.
- [60] A. M. Dziewonski and D. L. Anderson. Preliminary reference earth model. *Phys. Earth Planet. Interiors*, 25:297–356, 1981.
- [61] Hyper-Kamiokande Design Report. 2016.
- [62] Sandhya Choubey, Monojit Ghosh, and Dipyaman Pramanik. Sensitivity study of Protvino to ORCA (P2O) experiment: effect of antineutrino run, background and systematics. *Eur. Phys. J.*, C79(7):603, 2019.
- [63] A. V. Akindinov et al. Letter of Interest for a Neutrino Beam from Protvino to KM3NeT/ORCA. *Eur. Phys. J.*, C79(9):758, 2019.
- [64] CEPC-SPPC Study Group. CEPC-SPPC Preliminary Conceptual Design Report. 2. Accelerator. 2015.
- [65] M. G. Aartsen et al. A Search for Neutrino Point-Source Populations in 7 Years of IceCube Data with Neutrino-count Statistics. 2019.